PCCP

PAPER

View Article Online
View Journal | View Issue

Cite this: *Phys. Chem. Chem. Phys.*, 2014, **16**, 18375

Influence of nanosecond pulsed plasma on the non-enzymatic pathway for the generation of nitric oxide from L-arginine and the modification of graphite oxide to increase the solar cell efficiency†

Pankaj Attri,*[a] Ji Hoon Park,‡[a] Jitender Gaur,‡[b] Naresh Kumar,[a] Dae Hoon Park,[a] Su Nam Jeon,[a] Bong Sang Park,[a] Suresh Chand,[b] Han Sup Uhm[a] and Eun Ha Choi*[a]

Received 7th June 2014,
Accepted 14th July 2014

DOI: 10.1039/c4cp02514h

www.rsc.org/pccp

In this work, we demonstrated the action of nanosecond pulsed plasma (NPP) on the generation of nitric oxide (NO) from the non-enzymatic pathway and on the modification of graphite oxide (GO) sheets to increase polymer solar cells (PSCs) efficiency. NO is an important signal and an effector molecule in animals, which is generated from the enzyme-catalyzed oxidation of L-arginine to NO and L-citrulline. Hence, L-arginine is an important biological precursor for NO formation. Therefore, we developed a new non-enzymatic pathway for the formation of NO and L-citrulline using NPP and characterized the pathway using NO detection kit, NMR, liquid chromatography/capillary electrophoresis-mass spectrometry (LC/CE-MS) for both quantitative and qualitative bioanalysis. We then synthesized and modified the functional groups of GO using NPP, and it was characterised by X-ray photoelectron spectroscopy (XPS), confocal Raman spectroscopy, scanning electron microscopy (SEM), transmission electron microscopy (TEM) imaging, cathodoluminescence (CL) and work function using γ-FIB. Further, we also tested the power conversion efficiency of the PSCs devices with modified GO that is similar to the one obtained with poly(3,4-ethylenedioxythiophene):poly(styrenesulfonate) as HTL. This work is perceived to have great implications for inexpensive and efficient methodology for NO generation and modification of GO, which are applicable in materials from nanomaterials to biomolecules.

1. Introduction

Over the past several decades, many research groups have been keen to explore the phenomena of plasma in liquids.[1–4] The strong electric fields applied in liquids has provided various applications in chemistry, biology and physics.[5] Liquid electrical discharges typically include corona or corona-like, pulsed arcs and spark discharges.[5–8] Molecular oxygen, hydrogen and reactive species (RS) like nitric oxide (NO), hydrogen peroxide (H_2O_2), hydroxyl radical (OH), hydroperoxyl radicals (HO_2), hydrogen, and singlet oxygen have been generated by high voltage electrical discharges directly in water,[9–13] which along with their physical conditions have many practical applications, such as the inactivation of viruses, yeast, and bacteria,[14,15] efficient degradation of many organic compounds,[16–18] and the oxidation of several inorganic ions in water.[19] Also, high voltage electrical discharge processes have great applications in the field of green chemistry including organic compounds synthesis,[20–22] polymers synthesis,[23] nanomaterials synthesis[24] and biomedical engineering applications (surgery and skin treatment).[25]

Reactive oxygen species (ROS)[26,27] and reactive nitrogen species (RNS)[28,29] are conventional species thought to play an important role in many biological systems whereas, ROS and RNS created by the electrical discharges directly in liquid do not receive much attention. Nitric oxide (NO) biology has gained a widespread interest since mammals are capable of NO biosynthesis as established by nutrition and toxicology research conducted in the early 1980s.[30,31] The conversion of L-arginine to L-citrulline in the synthesis of NO catalyzed by nitric oxide synthase, which has a wide range of functions in cellular physiology, including cell signaling and host defense system,[32] has led to the development of methods to detect these amino acids in order to assay the enzymatic activities of NOS and other enzymes involved in NO synthesis.[33,34] An excellent study done by Nagase *et al.*[35] reveals the non-enzymatic pathway for the

[a] *Plasma BioScience Research Center/Department of Electrical and Biological Physics, Kwangwoon University, Seoul, Korea. E-mail: ehchoi@kw.ac.kr, chem.pankaj@gmail.com; Fax: +82-2-913-6187; Tel: +82-2-940-5236*

[b] *Council of Scientific and Industrial Research-National Physical Laboratory, Dr. K. S. Krishnan Marg, New Delhi-110012, India*

† Electronic supplementary information (ESI) available. See DOI: 10.1039/c4cp02514h

‡ These authors contributed equally to this work.

generation of NO by the reaction of H_2O_2 with L-arginine. The resin-supported iron(III) porphyrin for the generation of NO through oxidation of L-arginine using hydrogen peroxide has already been developed by Ray *et al.*[36] Hence, in this work we studied L-citrulline and NO production caused by point–point (point) and plane–plane (plane) electrodes under pulsed discharge for both quantitative and qualitative bioanalysis using liquid chromatography/capillary electrophoresis-mass spectrometry (LC/CE-MS), NMR and NO detection kit, respectively.

Solution processable graphene oxide (GO) is a new and recent dimension in polymer solar cells (PSCs), where it has emerged as a strong alternative to the PEDOT:PSS as HTL, owing to its non-corrosive character and optimum work function for enhanced hole collection at the ITO anode.[37–42] Hence, we synthesized GO by Hummer's methods[43,44] and modified the functional groups using NPP. Further, we used these modified GO as HTL in PSCs. To observe the effect of these modified GO sheets on PCE of PSCs, we used a cost-effective combination of low band gap donor polymer PTB7 and electron acceptor [6,6]-phenyl C61 butyric acid methyl ester ($PC_{61}BM$), instead of the costly $PC_{71}BM$, as the BHJ active layer, which has been reported to show PCE ~3% with PEDOT:PSS as HTL.[45]

2. Experimental section

2.1 Nanosecond pulsed plasma (NPP) in liquid using a Marx generator

In order to generate the nanosecond pulsed plasma in liquid, we employed the simplest and most widely used high voltage pulse generation device, the Marx generator. The basic principle of Marx generator involves the charging a set of parallel capacitors and then discharging them in series. Our Marx generator consisted of 5 stages. Each capacitor (a total of 5 capacitors) has a capacitance of 0.5 μF. This capacitor was connected with a 60 kΩ resistor in parallel. Every spark switch made from brass was located on the Lucite tube. The diameter and thickness of the Lucite tube were 100 mm and 4 mm, respectively. By going through the Lucite tube using screw, every spark switch was connected to the circuits. After charging the capacitors, switching was induced by generating the first spark gap, as shown in the schematic diagram in Fig. 1. For the experiment, we used two types of electrodes, the first was a point–point (point) electrode with a diameter of 2 mm and the second was a plane–plane (plane) electrode with a diameter of 10 mm. Both electrodes were made up of stainless steel of high relative stability even at elevated temperatures, which was located in a cylindrical tube. In this experiment, the distance of electrode was fixed at 6 mm, which was located in the cylindrical tube, as shown in Fig. 1. The length of cylindrical tube was 320 mm, the external diameter was 50 mm, and the inner diameter was 10 mm. For each different electrode type, the breakdown voltage and current were measured using a 1000:1 probe (Tektronix P6015A) and Rogowski coil (Pearson Current Monitor 411, output volts per ampere: 0.1), respectively. The voltage and current reached their peak values of 25 kV and 3.5 kA, respectively, for point–point electrode, whereas the voltage and current values for plane–plane electrodes were 22 kV and 3.6 kA, respectively. The breakdown energy was 0.104 J for point and 0.108 J for plane electrodes by integrating the

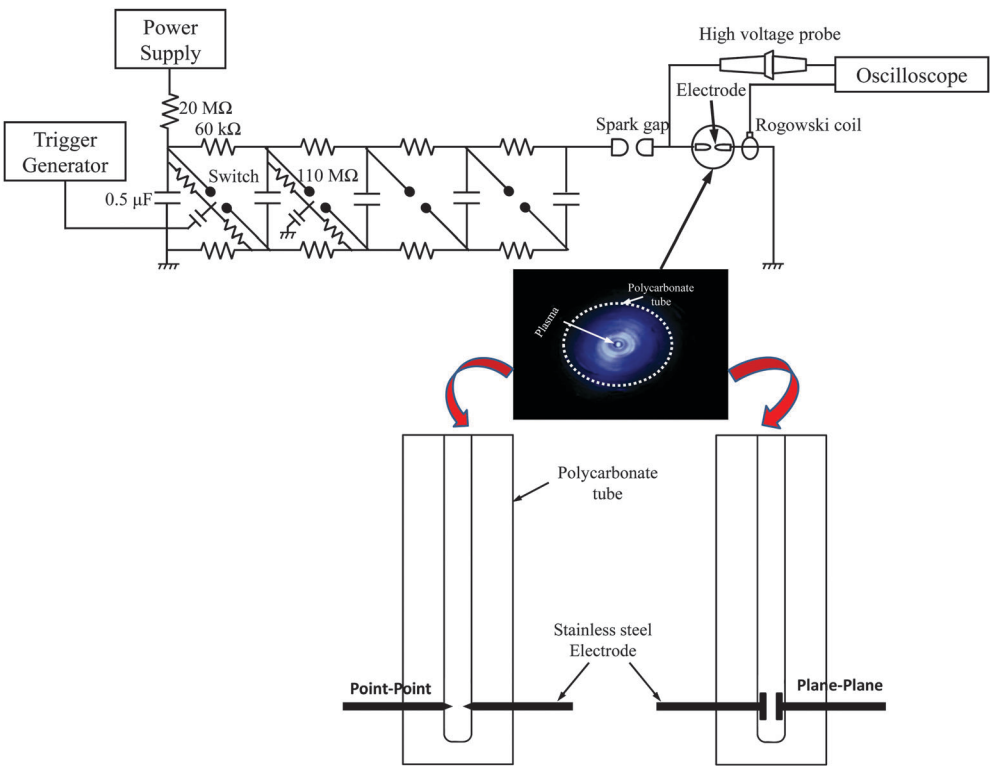

Fig. 1 Schematic diagram of the NPP device.

Table 1 Physical parameters of the NPP discharges in both electrodes

Electrodes	Peak voltage (kV)	Peak current (kA)	Breakdown voltage (kV)	Breakdown current (kA)	Breakdown time (ns)	Breakdown energy (J)
Point	25	3.5	14	0.6	500	0.104
Plane	22	3.6	10	0.7	600	0.108

product of breakdown voltage and current with respect to time during breakdown times. Moreover, the breakdown time for point and plane electrodes were 500 ns and 600 ns, respectively, as shown in Table 1. Further, we can see the single shot images using a pinhole camera (pinhole camera has a focal length of 32 mm and a pinhole diameter of 0.25 mm), as displayed in Fig. 1.

2.2 Materials

L-Arginine (Arg), graphite powder, H_2SO_4, $NaNO_3$, NaOH were supplied by Aldrich Chemical Co. (USA). All chemicals and reagents were used without any further purification. The concentrations of H_2O_2 were measured using an Amplex H_2O_2 assay kit (Invitrogen, Grand Island, NY, USA) and NO detection assay kit (Biovision, Milpitas, CA, USA), respectively, following the manufacturer's protocols.

2.3 Measurements

Quantitative analyses of amino acids were studied using liquid chromatography/capillary electrophoresis-mass spectrometery (LC/CE-MS) of Model Quattro LC Triple quadrupole mass spectrometer (Micromass & Waters), HP-1100 high performance liquid chromatography (Hewlett Packard) and HP-3D capillary electrophoresis (Hewlett Packard). The morphologies of the samples were observed under scanning electron microscopy (SEM, JEOL JSM-6360) and transmission electron microscopy (TEM, JEOL: JEM-1230) operating at 80–120 kV. The Raman spectra were measured at room temperature using a confocal Raman microscope (WITec, Alpha 300 R) with a 632.8 nm He–Ne laser. In order to obtain the Raman spectra for the GO sheets, the incident laser beam was focused onto the sample using a microscope objective (100×). The scattered light was collected by the same objective lens and dispersed by a grating and then detected by a charge-coupled device array detector. The high-resolution XPS experiments were performed on the PLS-8A1 undulator (U7) beam line equipped with a variable-included-angle plane-grating monochromator. Cathodoluminescence (CL) experiments were studied using MonoCL3 purchased from Gaton UK company. For CL measurements the control GO and treated GO samples were vacuum-dried at 30 °C on glass substrates.

2.4 Fabrication of polymer solar cell devices

The procedure for preparing PSCs in the configurations of ITO/PEDOT:PSS/PTB7:PC61BM/Al and ITO/GO/PTB7:PC61BM/Al is given below. ITO glass substrates were thoroughly cleaned with detergent followed by treating with different solvents in sequence *viz.*, acetone, trichloroethylene and isopropanol in an ultrasonic bath. The substrates were then cleaned by annealing at 150 °C in a vacuum oven for 20 min and subsequently exposing to the UV ozone for 10–15 min. PEDOT:PSS (Sigma Aldrich, USA, with 1.3% dispersion in water) and GO sheets (with 4th discharge of NPP or without discharge) were spin-coated on these cleaned substrates using a digital spin coater with optimized spin rates for a particular thickness. Furthermore, the substrates were dried at 140 °C for 30 min in the vacuum oven. Next, they were transferred into a glove box for the deposition of the active layer on the substrate using the spin cast technique, which required a mixture of PTB7:$PC_{61}BM$ in a chlorobenzene solvent with a concentration of 20 mg ml^{-1}. The spin-casted active layer was cured at 140 °C for 20 min under nitrogen atmosphere in the glove box. Finally, a shadow mask inside the thermal evaporator chamber having vacuum of $\sim 8 \times 10^{-6}$ mbar was used for depositing the aluminum electrodes of a thickness of 120 nm. The pixel device so prepared had an active area of ~ 0.075 cm^2. A Keithley 2420 source meter unit interfaced with a computer under tungsten halogen lamp illumination with an intensity of 1000 W m^{-2} was utilized for recording the current density–voltage (J–V) characteristics of the devices.

3. Result and discussion

We intended to explore the effect of NPP on the production of NO and modification of GO sheets. Therefore, we designed a Marx generator to produce and characterize the NPP in liquid. During discharge in liquids, electrons were initially accelerated in the applied field and acquired sufficient energy to ionize or excite water molecules. The breakdown energy as displayed in Table 1, was calculated to be ≈ 0.10 J by integrating the breakdown voltage and current. Fig. 2 shows the emission spectrum between 200 and 1100 nm from NPP in distilled water using both electrodes. The excited states of atomic hydrogen in the Balmer series appeared as H_α at 656.28 nm, H_β at 486.13 nm, and H_γ at 434.04 nm, and atomic oxygen ($3p^5P^0 \rightarrow 3s^5S^0$ at 777.5 nm) was detected in the emission spectra, while the molecular band at 306.4 nm ($A^2\Sigma^+ \rightarrow X^2\Pi$) was attributed to that of the hydroxyl (OH) radicals. Further, emission lines were observed for a molecular NO β, γ system between 200 and 250 nm and a superoxide anion (O_2^*) at 245 nm.[46,47] Additionally, we studied the concentration of NO and H_2O_2 for both point and plane electrodes as shown in Fig. S1 (ESI†). It was found out that the level of H_2O_2 was highest for plane electrode as compared to the point electrode. On the contrary, it was revealed that the concentration of NO radicals was maximum in point electrode as compared to the plane electrode. Hence, it was stated that the concentration of H_2O_2 and NO was different for both electrodes. We then examined the temperature and pH after discharges, and the results are as depicted in Fig. S2 (ESI†). No change in temperature and pH of the solution was

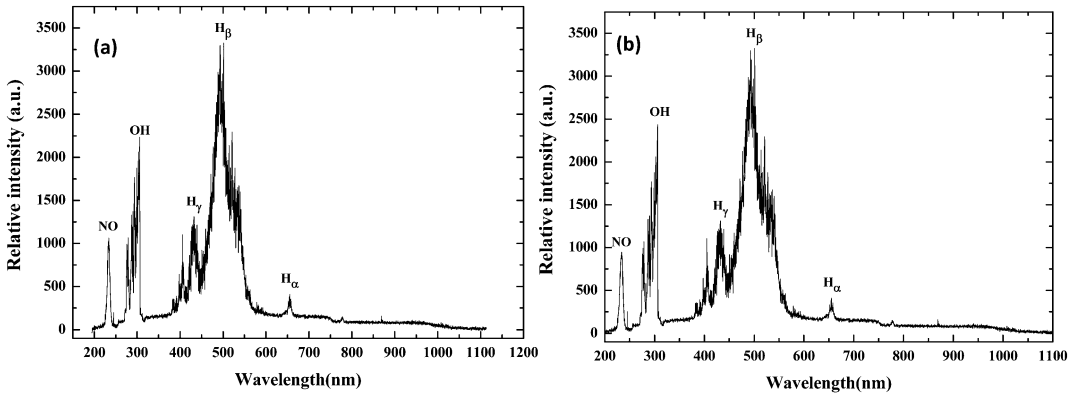

Fig. 2 The emission spectrum between 200 and 1100 nm from NPP in distilled water using both electrodes.

noticed after discharges using both electrodes. Different levels of ROS and RNS species lead to different levels of modification of the amino acids and GO sheets.

3.1 L-Citrulline and NO generation from L-arginine using NPP

The generation of NO from L-arginine, which occurs exclusively through the catalytic action of NOS has been universally accepted.[48] Hence, this study aims to propose a new non-enzymatic pathway for NO synthesis from L-arginine in solution. The high plasma concentration of NO_X in dialysis patients was suggested as a result of an increased production of NO in addition to a decreased renal clearance.[49] It has been found that the production rate of NO in hemodialysis patients as calculated from the increased levels of plasma NO_X during hemodialysis was significantly higher than that of healthy controls.[35] The current study suggests one possible mechanism for the elevated plasma as the presence of a peroxidative state in patients with renal failure is commonly known.[35] As it is clear from Fig. S1 (ESI†), the NPP plasma can produce H_2O_2 and NO in water. Moreover, the emission spectra show that both point and plane electrodes can produce the NO and OH radicals. Additionally, Nagase *et al.*[35] can generate NO by the reaction of H_2O_2 with L-arginine from a non-enzymatic pathway. To make this as the standard route for the generation of NO and L-citrulline, we treated L-arginine with the nanosecond pulsed plasma as illustrated in Scheme 1. Next, we determined the concentration of NO and H_2O_2 in the L-arginine solution after the treatment, as shown in Fig. 3. We observed that the H_2O_2 generation was decreased after the treatment in L-arginine solution as compared to water alone for both electrodes. However, the generation of the NO radical increased as compared to water alone after the treatment of L-arginine with NPP for both electrodes. These results indicate that the amount of NO released from L-arginine through non-enzymatic reaction

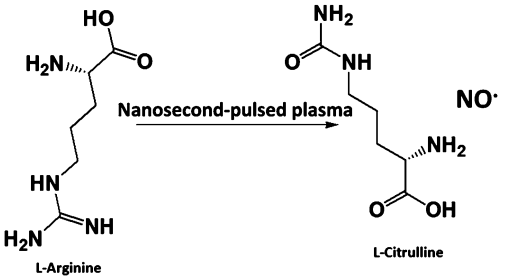

Scheme 1 Generation of L-citrulline and NO from L-arginine using NPP.

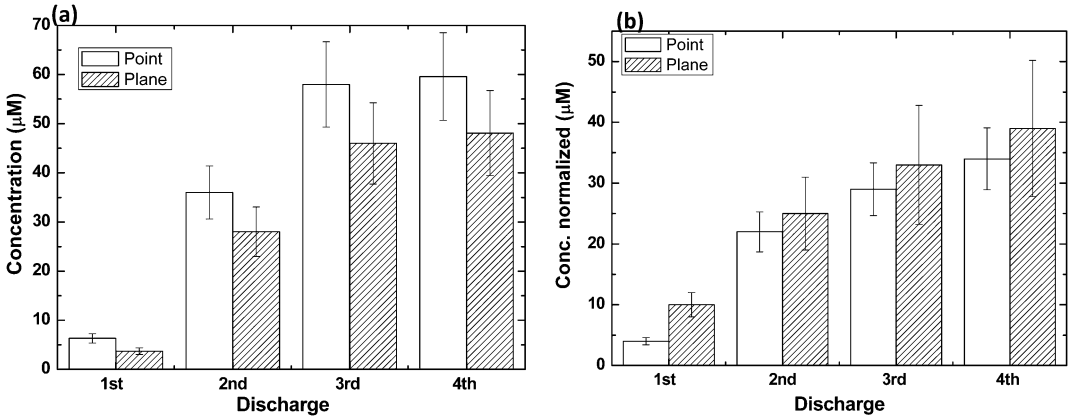

Fig. 3 (a) NO and (b) H_2O_2, concentration changes in physiological solutions exposed to point and plane electrodes in L-arginine water solution at different number of discharges.

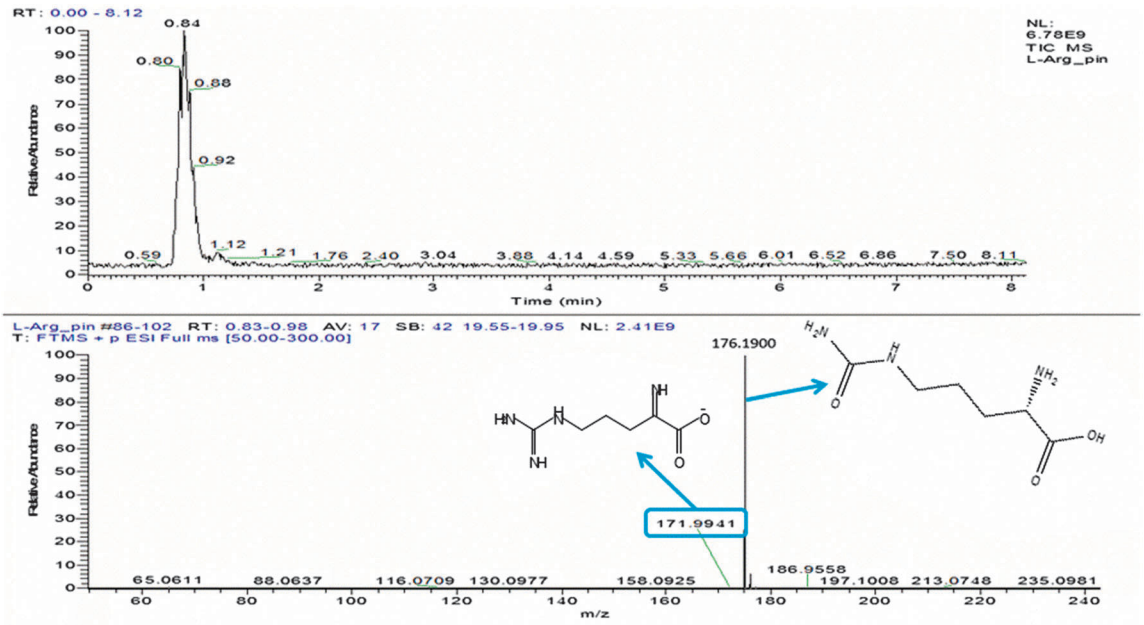

Fig. 4 Liquid chromatography/capillary electrophoresis-mass spectrometry (LC/CE-MS)-based qualitative bioanalysis of L-arginine + point electrode.

depends on the hydrogen peroxide concentration created during NPP discharge in the solution. The nitrogen atom of NO could be derived from either the guanidino or the amino group.

Moreover, as the number of discharge was increased, the production of NO sequentially increased and the concentration of the H_2O_2 decreased as compared to the discharges in water alone. The possible mechanism could be the cleavage of nitrogen from the amino by hydrogen peroxide. Further, to confirm the formation of L-citrulline from the above reaction, we used liquid chromatography/capillary electrophoresis-mass spectrometry (LC/CE-MS) for both quantitative and qualitative bioanalysis after the 4th discharge. ROS created by plasma reacted with L-arginine and fragmented into either higher molecular weight or lower molecular weight products which depended on the level of ROS created by different electrodes. Therefore, to investigate these types of changes, we studied the quantitative amino acid analysis showing 164.200 μg ml^{-1} as the control mass for L-arginine, which after the point discharge is 167.814 μg ml^{-1} and 165.379 μg ml^{-1} after the plane discharge, as shown in Table S1 (ESI†). Hence, the mass increases after the discharge reveals that the L-arginine is converted into a higher molecular weight product after the discharge. This data reveals that L-arginine is oxidized and converted to L-citrulline after the discharge. Further, in order to learn more about product formation after the reaction with NPP, we performed the qualitative analysis using LC/CE-MS, as displayed in Fig. 4 and 5, Fig. S3 (ESI†). It is shown from Fig. 4 and 5, Fig. S3 (ESI†) that new species are formed after discharge. Peaks at 176.1900 *m*/*z* (M + H) for point discharge and 176.1901 *m*/*z* (M + H) for plane discharge were observed, which indicates the formation of L-citrulline, while the 175.1188 *m*/*z* (M + H) peak indicates the L-arginine solution before NPP discharges. Further, we separated the L-citrulline as per a reported procedure[36] and obtained the proton NMR spectra that confirmed the formation of L-citrulline. Peaks at 3.64–3.62 (t), 3.04–3.01 (t), 1.78–1.75 (m) and 1.49–1.43 (m) clearly indicated the formation of L-citrulline with 65% yield, and the % yield was also found to be same for both electrodes (as shown in Fig. S4, ESI†). Further, we also studied the modification of the GO structure after the plasma discharge.

3.2 Characterization and morphology of synthesized GO and modified GO

The characterization and morphology of synthesized GO and modified GO was carried out using X-ray photoelectron spectroscopy (XPS), confocal Raman spectroscopy, scanning electron microscopy (SEM), transmission electron microscopy (TEM) imaging, cathodoluminescence (CL) and variation of the work function of GO with or without plasma using γ-FIB. GO sheets possess oxygen functionalities as their XPS survey scan shows peaks corresponding to C 1s, as illustrated in Fig. S5 (ESI†). The binding energies were corrected by taking the C 1s core level at 284.6 eV for all samples.[50,51] Carbon 1s XPS spectra show signals at 284.6, 286.02, 287.06 and 289.04 eV, respectively, which corresponds to the C–C, C–O, C═O and COO functional groups in GO.[52,53] Further, the comparative analysis of relative intensities of these signals showed that the alcohol functional group are dominant as compared to the carbonyl and carboxylic functional groups. Whereas, after the 4th discharge using the point electrode, the carbonyl group has more intensity than the carboxyl and alcohol functional groups, which shows the C–O was converted to C═O after treatment. While for the 4th plane electrode discharge the carboxyl functional group has more intensity as compared to the carbonyl and alcohol functional groups. This shows the different extents of oxidation after the discharge in using point and plane

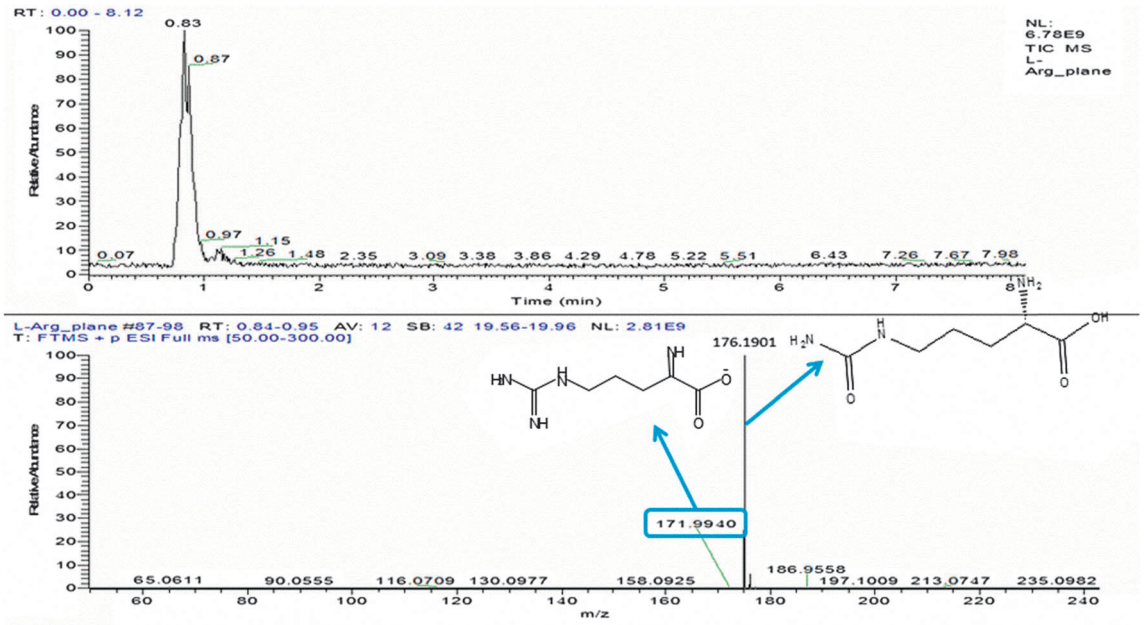

Fig. 5 Liquid chromatography/capillary electrophoresis-mass spectrometry (LC/CE-MS)-based qualitative bioanalysis of L-arginine + plane electrode.

electrode, which leads to different modifications. In additional, we studied the Raman spectra, where two bands were observed at 1350 and 1607 cm^{-1}, respectively. It is postulated that these bands correspond to the G (graphitic) and D (disordered) bands of the GO sheets, as shown in Fig. S6a (ESI†). For GO sheets, the ratio of intensities of D and G bands was found to be greater than one, *i.e.*, $I_D/I_G > 1$, which is characteristic of the oxidized edges of graphene developed in GO sheets whereas, no significant difference in Raman data was observed after the treatment (data not shown).

The morphology of the GO sheets was observed by SEM and TEM imaging, as displayed in Fig. S6b and c (ESI†). The magnified image of Fig. S6b (ESI†) clearly demonstrates that partial circular disc-like structures consisted of graphene planes and are attached through their radial edges. These all clearly appear as partial circular discs with a diameter in the range of 1 to 2 μm. The homogeneous morphology of the GO sheets was established from Fig. S6b (ESI†). Further, a uniform morphology of GO sheets is well illustrated from the TEM images as shown in Fig. S6c (ESI†), whereas no significant difference in morphology was observed after the treatment with both electrodes (data not shown). Additionally, the measurement of the work function of a GO before and after the NPP treatment with different electrodes is an important factor to determine the efficiency of the solar cell.[54] The work function was calculated using the γ-FIB system; the results are shown in Fig. 6a and Table S2 (ESI†). Through this, we could calculate the work function of the GO sheet, which was found to be 10.63 eV, whereas after the point electrode treatment, the work function was 8.56 eV. For the plane electrode, the work function was found to be 9.21 eV. Thus, we can see that after the NPP treatment, the work function decreases as compared to the untreated GO sheets.

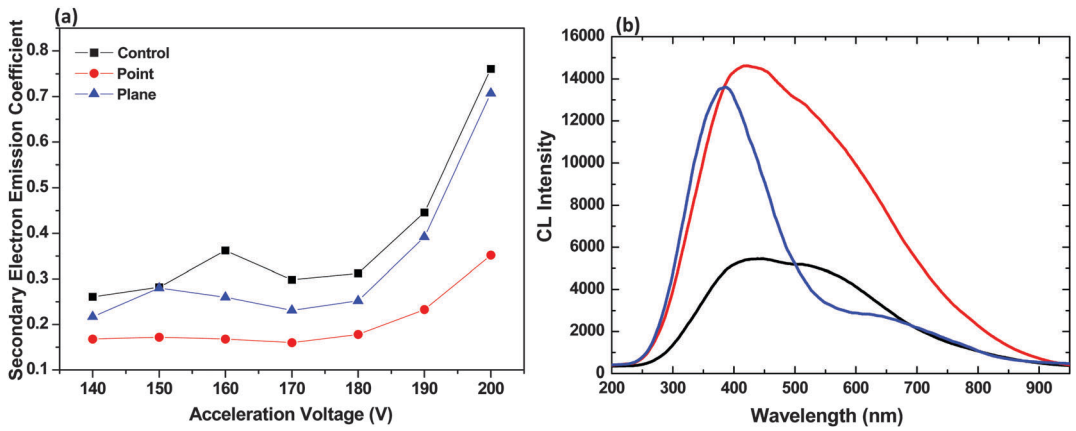

Fig. 6 (a) Secondary electron emission coefficient and (b) cathodoluminescence (CL) spectrum intensity of GO (black), GO treated with point electrode plasma (red) and GO treated with point electrode plasma (blue).

Further, we studied the cathodoluminescence (CL)[54] for GO both before and after the NPP treatment, as displayed in Fig. 6b. Here, the results are also as expected and correlated with the above experimental data. After the treatment, GO sheets showed the red and blue shift with an increase in intensity. In the presence of point electrode plasma, the red shift was observed with a broad peak, whereas for the plane electrode plasma, we observed quenching with the blue shift as compared to the point electrode discharge. The difference in spectra of GO sheets before and after treatment in the presence of different electrodes reveals that there is a change in the crystal polymorphs of the GO sheets after the treatment. Hence, CL data also support our results that there is a considerable change in the GO structure after the NPP treatment, which in turn modifies its physical and optical properties to a great extent.

3.3 Solar cell application of GO

High oxygen functionalization and optimum band gap are the key properties for the utilization of GO as HTL in PSCs to improve the hole transport at the anode with adequate blocking of electrons.[37–42,55] From the above detailed characterization of these GO sheets, it was established that they are highly rich in oxygen functionalities. The findings of all the above mentioned characterization indicates the utility of GO sheets before and after treatment as HTL in PSCs. In fact, the performance of these GO sheets as an alternative HTL to PEDOT:PSS was studied by fabricating PSCs using donor conjugated polymer PTB7 and electron acceptor $PC_{61}BM$. To compare the effects of PEDOT:PSS and GO sheets as HTL, the devices were fabricated in two configurations *viz.*, ITO/PEDOT:PSS/PTB7:$PC_{61}BM$/Al and ITO/GO/PTB7:$PC_{61}BM$/Al, respectively. The current density and voltage (J–V) characteristics of these devices are shown in Fig. S7 (ESI†). The open circuit voltage (V_{oc}), short circuit current density (J_{sc}), fill factor (FF), PCE, series resistances RS (Ω) and shunt resistance RSH (Ω) values for each set of device are given in Table 2. It is explicit from Table 2 that the device of the GO thickness of ~2 nm has PCE of about 2.5% and FF at 39.7%, while after the point discharge the PCE was ~3.0% with FF at 41.2%; the PCE was ~2.9% with FF at 38.7% after the plane electrode discharge. This shows that the increase in the PCE of the solar cells after the treatment. These results are very well correlated with literature results, where after the O_2 plasma treatment on GO, we observed an increase in cell efficiency.[40] However, the structural properties were changed much after the treatment from both point and plane electrode; however, the increase in efficiency was found to be almost the same for both electrodes.

Table 2 Device parameters from PTB7:$PC_{61}BM$ PSCs measured under illumination intensity of 1000 W m^{-2}

HTL layer	J_{sc} (mA cm^{-2})	V_{oc} (V)	FF (%)	PCE (%)	RS (Ω)	RSH (Ω)
PEDOT:PSS	10.39	0.74	39.2	3.0	23.0	147.1
GO	8.40	0.74	39.7	2.5	24.2	190.6
GO (point)	9.84	0.75	41.2	3.0	25.9	165.3
GO (plane)	10.2	0.74	38.7	2.9	28.3	144.8

4. Conclusion

In conclusion, we demonstrated an innovative method for the conversion of L-arginine to NO and L-citrulline from non-enzymatic pathway in solution. The formation of NO and L-citrulline was studied using NO kit, liquid chromatography/capillary electrophoresis-mass spectrometry (LC/CE-MS) for both quantitative and qualitative bioanalysis and NMR. Additionally, we modified the GO sheets to different extents using different electrodes and characterized them by X-ray photoelectron spectroscopy (XPS), confocal Raman spectroscopy, scanning electron microscopy (SEM), transmission electron microscopy (TEM) imaging, cathodoluminescence (CL) and work function using γ-FIB. Further, these modified GO were used as HTL in PSCs, where the PCE of the cell increased after the discharge using NPP, while the differences in efficiency were found to be negligible between two electrodes. This work provides a new scope for nanosecond pulsed plasma.

Acknowledgements

We dedicated this work to the Late Prof. Hee-Myung Shin, Emeritus Professor for their contribution towards plasma physics. This work has been supported by a National Research Foundation of Korea (NRF) grant funded by the Ministry of Science, ICT and Future Planning (MSIP) (NRF-2010-0027963 and 20120009639). This work has also been partially supported by Kwangwoon University 2014. JG and SC are thankful to DST, Govt. of India, for providing financial support under the India–UK joint initiative project titled "Advancing the efficiency and production potential of excitonic solar cells (APEX)." We also thank Mr Vishal Bharti and Dr Gauri D Sharma for their valuable help.

References

1 A. Starikovskiy, Y. Yang, Y. I. Cho and A. Fridman, *Plasma Sources Sci. Technol.*, 2011, **20**, 024003.
2 P. Bruggeman and P. Leys, *J. Phys. D: Appl. Phys.*, 2009, **42**, 053001.
3 P. Vanraes, A. Nikiforov and C. Leys, *J. Phys. D: Appl. Phys.*, 2012, **45**, 245206.
4 W. An, K. Baumung and H. Bluhm, *J. Appl. Phys.*, 2007, **101**, 053302.
5 D. Dobrynin, Y. Seepersad, M. Pekker, M. Shneider, G. Friedman and A. Friedman, *J. Phys. D: Appl. Phys.*, 2013, **46**, 105201.
6 M. Sato, *Plasma Sources Sci. Technol.*, 2008, **17**, 024021.
7 S. Shiina, T. Ohshima and M. Sato, *Biotechnol. Prog.*, 2004, **20**, 1528–1533.
8 P. Sunka, V. Babicky, M. Clupek, P. Lukes, M. Simek, J. Schmidt and M. Cernak, *Plasma Sources Sci. Technol.*, 1999, **8**, 258–265.
9 M. J. Kirkpatrick and B. R. Locke, *Ind. Eng. Chem. Res.*, 2005, **44**, 4243–4248.
10 R. A. Davies and A. Hickling, *J. Chem. Soc., Faraday Trans.*, 1952, 3595–3602.

11 A. A. Joshi, B. R. Locke, P. Arce and W. C. Finney, *J. Hazard. Mater.*, 1995, **41**, 3–30.
12 A. Hickling, *Mod. Aspects Electrochem.*, 1971, **6**, 329–373.
13 M. Sahni and B. R. Locke, *Plasma Processes Polym.*, 2006, **3**, 342–354.
14 A. J. H. Sale and W. A. Hamilton, *Biochim. Biophys. Acta*, 1967, **148**, 781–788.
15 S. Jayaram, G. S. Castle and A. Margaritis, *Biotechnol. Bioeng.*, 1992, **40**, 1412–1420.
16 Y. Z. Wen and X. Z. Jiang, *Plasma Chem. Plasma Process.*, 2001, **21**, 345–354.
17 D. C. Johnson, V. A. Shamamian, J. H. Callahan, F. S. Denes, S. O. Manolache and D. S. Dandy, *Environ. Sci. Technol.*, 2003, **37**, 4804–4810.
18 A. K. Sharma, G. B. Josephson, D. M. Camaioni and S. C. Goheen, *Environ. Sci. Technol. Lett.*, 2000, **34**, 2267–2272.
19 B. Benstaali, D. Moussa, A. Addou and J. L. Brisset, *Eur. Phys. J.: Appl. Phys.*, 1998, **4**, 171–179.
20 S. L. Miller, *J. Am. Chem. Soc.*, 1955, **77**, 2351–2361.
21 K. Harada and S. Suzuki, *Nature*, 1977, **266**, 275–276.
22 K. Harada and T. Iwasaki, *Nature*, 1974, **250**, 426–429.
23 S. K. Sengupta, U. Sandhir and N. Misra, *J. Polym. Sci., Part A: Polym. Chem.*, 2001, **39**, 1584–1588.
24 H. Lange, M. Sioda, A. Huczko, Y. Q. Zhu, H. W. Kroto and D. R. M. Walton, *Carbon*, 2003, **41**, 1617–1623.
25 K. R. Stalder, J. Woloszko, I. G. Brown and C. D. Smith, *Appl. Phys. Lett.*, 2001, **79**, 4503–4505.
26 S. S. Grant, B. B. Kaufmann, N. S. Chand, N. Haseley and D. T. Hung, *Proc. Natl. Acad. Sci. U. S. A.*, 2012, **109**, 12147–12152.
27 T. Finkel and N. J. Holbrook, *Nature*, 2000, **408**, 239–247.
28 F. Q. Guo, M. Okamoto and N. M. Cawford, *Science*, 2003, **302**, 100–103.
29 J. S. Isenberg, L. A. Ridnour, E. M. Perruccio, M. G. Espey, D. A. Wink and D. D. Roberts, *Proc. Natl. Acad. Sci. U. S. A.*, 2005, **102**, 13141–13146.
30 L. C. Green, K. Ruiz de Luzuriaga, D. A. Wagner, W. Rand, N. Istfan, V. R. Young and S. R. Tannenbaum, *Proc. Natl. Acad. Sci. U. S. A.*, 1981, **78**, 7764–7768.
31 L. Castillo, L. Beaumier, A. M. Ajami and V. R. Young, *Proc. Natl. Acad. Sci. U. S. A.*, 1996, **93**, 11460–11465.
32 S. M. Morris, *J. Nutr.*, 2007, **137**, 1602S.
33 M. Kameyaa and Y. Asanoa, *Enzyme Microb. Technol.*, 2014, **57**, 36–41.
34 M. Knipp and M. Vasak, *Anal. Biochem.*, 2000, **286**, 257–264.
35 S. Nagase, K. Takemura, A. Ueda, A. Hirayama, K. Aoyagi, M. Kondoh and A. Koyama, *Biochem. Biophys. Res. Commun.*, 1997, **233**, 150–153.
36 M. Mukherjee and A. R. Ray, *J. Mol. Catal. A: Chem.*, 2007, **266**, 207–214.
37 S. S. Li, K. H. Tu, C. C. Lin, C. W. Chen and M. Chhowalla, *ACS Nano*, 2010, **6**, 3169–3174.
38 I. P. Murray, S. J. Lou, L. J. Cote, S. Loser, C. J. Kadleck, T. Xu, J. M. Szarko, B. S. Rolczynski, J. E. Johns, J. Huang, L. Yu, L. X. Chen, T. J. Marks and M. C. Hersam, *J. Phys. Chem. Lett.*, 2011, **2**, 3006–3012.
39 J. M. Yun, J. S. Yeo, J. Kim, H. G. Jeong, D. Y. Kim, Y. J. Noh, S. S. Kim, B. C. Ku and S. I. Na, *Adv. Mater.*, 2011, **23**, 4923–4928.
40 D. Yang, L. Zhou, L. Chen, B. Zhao, J. Zhang and C. Li, *Chem. Commun.*, 2012, **48**, 8078–8080.
41 Y. Gao, H. L. Yip, S. K. Hau, K. M. Malley, N. C. Cho, H. Z. Chen and A. K. Y. Jen, *Appl. Phys. Lett.*, 2010, **97**, 203306.
42 J. Liu, Y. H. Xue, Y. X. Gao, D. S. Yu, M. Durstock and L. M. Dai, *Adv. Mater.*, 2012, **24**, 2228–2233.
43 W. S. Hummers and R. E. Offeman, *J. Am. Chem. Soc.*, 1958, **80**, 1339.
44 B. J. Li and H. Q. Cao, *J. Mater. Chem.*, 2011, **21**, 3346–3349.
45 W. Chen, T. Xu, F. He, W. Wang, C. Wang, J. Strzalka, Y. Liu, J. Wen, D. J. Miller, J. Chen, K. Hong, L. Yu and S. B. Darling, *Nano Lett.*, 2011, **11**, 3707–3713.
46 C. Miron, M. A. Bratescu, N. Saito and O. Takai, *Curr. Appl. Phys.*, 2011, **11**, S154–S156.
47 P. Attri, P. Venkatesu, N. Kaushik and E. H. Choi, *RSC Adv.*, 2012, **2**, 7146–7155.
48 R. M. J. Palmer and S. Moncada, *Biochem. Biophys. Res. Commun.*, 1989, **158**, 348–352.
49 A. Amore, R. Bonaudo, D. Ghigo, M. Arese, C. Costamagna, P. Cirina, B. Gianoglio, L. Perugini and R. Coppo, *J. Am. Soc. Nephrol.*, 1995, **6**, 1278–1283.
50 R. Li, X. Tao and X. Li, *J. Mater. Chem.*, 2009, **19**, 983–987.
51 R. Li, L. Bao and X. Li, *CrystEngComm*, 2011, **13**, 5858–5862.
52 D. V. Kosynkin, A. L. Higginbotham, A. Sinitskii, J. R. Lomeda, A. Dimiev, B. K. Price and J. M. Tour, *Nature*, 2009, **458**, 872–876.
53 J. Peng, W. Gao, B. K. Gupta, Z. Liu, R. R. Aburto, L. Ge, L. Song, L. B. Alemany, X. Zhan, G. Gao, S. A. Vithayathi, B. A. Kaipparettu, A. A. Marti, T. Hayashi, J. J. Zhu and P. M. Ajayan, *Nano Lett.*, 2012, **12**, 844–849.
54 J. H. Choi, C. G. Son, Y. J. Hong, B. C. Park, H. S. Uhm and E. H. Choi, *Adv. Nat. Sci.: Nanosci. Nanotechnol.*, 2010, **1**, 045014.
55 V. Gupta, N. Chaudhary, R. Srivastava, G. D. Sharma, R. Bhardwaj and S. Chand, *J. Am. Chem. Soc.*, 2011, **133**, 9960–9963.

